Nuclear Engineering and Technology xxx (xxxx) xxx

Contents lists available at ScienceDirect

Nuclear Engineering and Technology

journal homepage: www.elsevier.com/locate/net

Original Article

Molybdenum release from high burnup spent nuclear fuel at alkaline and hyperalkaline pH

Sonia García-Gómez [a], Javier Giménez [a,*], Ignasi Casas [a], Jordi Llorca [a], Joan De Pablo [a,b], Albert Martínez-Torrents [b], Frederic Clarens [b], Jakub Kokinda [b], Luis Iglesias [b], Daniel Serrano-Purroy [c]

[a] Department of Chemical Engineering, EEBE and Barcelona Research Center in Multiscale Science and Engineering, Universitat Politècnica de Catalunya (UPC), Eduard Maristany, 10-14, 08019, Barcelona, Spain
[b] EURECAT, Centre Tecnològic de Catalunya, Plaça de la Ciència 2, 08243, Manresa, Spain
[c] European Commission, Joint Research Centre (JRC), Karlsruhe, Germany

ARTICLE INFO

Keywords:
Spent nuclear fuel
Molybdenum
Metallic inclusions
Hyperalkaline conditions
Instant release fraction
X-ray photoelectron spectroscopy

ABSTRACT

This work presents experimental data and modelling of the release of Mo from high-burnup spent nuclear fuel (63 MWd/kgU) at two different pH values, 8.4 and 13.2 in air. The release of Mo from SF to the solution is around two orders of magnitude higher at pH = 13.2 than at pH = 8.4. The high Mo release at high pH would indicate that Mo would not be congruently released with uranium and would have an important contribution to the Instant Release Fraction, with a value of 5.3%.

Parallel experiments with pure non irradiated Mo(s) and XPS determinations indicated that the faster dissolution at pH = 13.2 could be the consequence of the higher releases from metallic Mo in the fuel through a surface complexation mechanism promoted by the OH^- and the oxidation of the metal to Mo(VI) via the formation of intermediate Mo(IV) and Mo(V) species.

1. Introduction

Spent nuclear fuel (SF) contains a significant amount of Mo due to a high fission yield of several Mo isotopes [1]. The Mo content has an important impact on the SF chemistry, which in turn may affect the radionuclide release from SF in a repository environment. Mo is found both in the SF matrix and in segregated metallic particles with metals such as Ru, Rh, Tc and Pd [1,2], such metallic inclusions were observed both in the grain boundaries and inside the grains [3] and seem to be precipitating when the Mo concentration in the fuel is relatively high [1]. Since the oxygen potential of Mo/MoO_2 is very similar to that of uranium dioxide, the excess oxygen created during fission is neutralized by the oxidation of metallic Mo to Mo(IV), buffering the oxidation of uranium dioxide [2,4]. The Mo(IV) formed by the oxidation seems to be inserted in the cationic positions of the UO_2 crystal lattice [5]. Molybdenum is present in the fuel, therefore, with at least two different oxidation states, which is relevant for the release of Mo when the fuel is in contact with groundwaters. If it is mainly in its metallic form it would be expected to be non-congruently released with uranium, but if Mo is inserted in the UO_2 crystal lattice as Mo(IV) it would be expected to be released congruently with uranium as the UO_2 matrix dissolves. In addition to the Mo(0) and Mo(IV) oxidation states, a portion of Mo oxidized to Mo(VI) during the handling of the fuel should also be considered [5], Mo at this oxidation state would rapidly be released to the groundwaters.

The presence of Mo in different oxidation states and in different sources in the fuel difficults the prediction of the release of Mo to groundwaters. For example, a Mo release higher than the expected considering the uranium release was found in experiments with different fuels, indicating that Mo was segregated from uranium and contributed to the Instant Release Fraction (IRF) [6–8]. However, in other experiments the behaviour of Mo was different depending on the fraction of the fuel dissolved, with a congruent release with uranium from the powdered center of a pellet (CORE experiments) and a higher release from the powdered rim of a pellet (OUT experiments) [9–11].

Such experiments were carried out at slightly alkaline pH, but the

* Corresponding author. Department of Chemical Engineering, EEBE and Barcelona Research Center in Multiscale Science and Engineering, Universitat Politècnica de Catalunya, Eduard Maristany, 10-14, 08019, Barcelona, Spain.
E-mail address: francisco.javier.gimenez@upc.edu (J. Giménez).

https://doi.org/10.1016/j.net.2023.08.024
Received 25 April 2023; Received in revised form 10 August 2023; Accepted 14 August 2023
Available online 15 August 2023

Table 1
Irradiation parameters of the samples used in this work.

Fuel properties	
Reactor type	PWR
^{235}U enrichment (weight%)	3.95
Average grain size (μm)	6.4
Fission Gas Release (FGR) (%)	13.6
Average BU (GWd t_{HM}^{-1})	60
Local BU (GWd t_{HM}^{-1})	63
Average Linear Power Density (W cm^{-1})	255
Cooling time (years)	15

Table 2
Characteristics of the samples used in this work. The outer diameter of the segments was 9.1 ± 0.1 mm, the exposed surface 546 ± 10 mm^2 and the S/V ratio 9.1 ± 0.2 mm^{-1}

Segment	pH = 8.4	pH = 13.2
Length (mm)	4.3 ± 0.1	3.5 ± 0.1
Weight with cladding (g)	3.541 ± 0.001	2.768 ± 0.001
Weight without cladding (g)[a]	2.62 ± 0.05	2.10 ± 0.05

[a] The weight of the pellet without cladding was estimated from the ratio pellet to cladding obtained after complete dissolution of a pellet.

design of a high-level nuclear waste repository includes materials based on concrete, due to both its adequate structural properties and its capacity to retard radionuclides release [12,13]. In this sense, it is necessary to take into account that the interaction of concrete materials with groundwater results in significant alterations in the groundwater composition, in particular, high pH (that can be even higher than 13) and high calcium and silicate concentrations [14].

The aim of this work is to show the variation of the Mo release from high-burnup SF at two different pH values and to deduce both the localization in the fuel and the oxidation state of the Mo released to the solution as a function of time. In order to understand the results obtained, the dissolution rate of Mo(s) was studied in the alkaline region under oxidizing conditions by using a thin-film continuous flow-through reactor, and X-ray Photoelectron Spectroscopy was used in order to determine the variation of the Mo oxidation state during the experiments.

2. Experimental

2.1. Solids

The dissolution experiments were carried out with a PWR high-burnup SF. The main irradiation parameters of the fuel are shown in Table 1 while the characteristics of the segments used in the experiments are summarized in Table 2. The samples were cladded segments cut using a low speed saw in absence of a cooling liquid from the center of a pellet, without the space between pellets [6].

Mo(s) powder with a mean particle size of <5 μm was supplied by Goodfellow. The specific surface area of the solid was determined by the Brunauer, Emmett, Teller (BET) method (Micromeritics ASAP 2020) based on adsorption/desorption isotherms of nitrogen at room temperature. The specific surface area determined was 0.282 ± 0.002 $m^2\ g^{-1}$.

2.2. Leaching solutions and experimental procedure

2.2.1. Spent nuclear fuel

The two leaching solutions used in the SF dissolution experiments had different pH, 8.3 and 13.2. The leaching solution at pH = 8.3 simulated a $1{\cdot}10^{-3}$ mol dm^{-3} bicarbonate groundwater and the solution at pH = 13.2 simulated the pH of the pore water composition in the cement buffer after the dissolution of alkaline oxides [15]. The pH of this water was monitored during five months before the start of the experiments and the measured pH was 13.2 ± 0.1 during the last three months, when the solutions were considered suitable for the experiments. No formation of precipitates was observed during the five months.

The experiments were performed in air and in a hot cell temperature of 25 ± 5 °C. The fuel segments were submerged in 50 cm^3 of the leaching solution under continuous stirring. After each predetermined time interval, the complete solution was taken out of the reactor and substituted by fresh solution. This procedure was carried out in order to prevent the precipitation of secondary solid phases during the experiments. Aliquots of the solution were acidified with HNO_3 and analysed by ICP-MS. ICP-MS analyses were performed using a Thermo ELEMENT XP instrument (Thermo Electron Corporation, Germany). Calibration curves were produced using a series of dilutions of certified multi-element standard solutions in the concentration range of the major elements in solution. Co, In, Ho and Th were used as internal standards in the sample measurements. The molybdenum moles included in this work were determined from isotopic data from Mo-95, Mo-97, Mo-98, and Mo-100. The Mo concentration was calculated from these isotopes and after the correction considering the presence of possible natural interferences, and correspond to fission molybdenum produced in the fuel [16]. Mo-92, Mo-94 and Mo-96 were not considered in the determination of the Mo cumulative moles in this work. In this sense, the possible release of molybdenum from the cladding or from the crud on the cladding was not considered in this work.

2.2.2. Non-irradiated Mo(s)

All solutions were prepared using Milli-Q water and contained 1.10^{-3} mol dm^{-3} of $NaHCO_3$ (Sigma Aldrich) to simulate the composition of a groundwater in a granitic environment. The range of pH studied was from 9 to 13.5. The desired value of pH in the test solution for each experiment was adjusted by adding NaOH (supplied by Sigma Aldrich). The pH was measured with a pH meter from Orion, model 720A and was daily calibrated with three pH standard buffer solutions from Panreac (pH 7, 9 and 13). The ionic strength of each solution was maintained constant and equal to 0.1 M (with the exception of pH 13.5) by using the required amount of sodium perchlorate (Sigma Aldrich). The solutions were continuously bubbled with synthetic air (21% O_2(g) and free of CO_2(g)) and the experiments were performed at room temperature.

The continuous flow-through thin solid layer reactor used in this work is described in detail in Ref. [17]. Briefly, 0.03 g of Mo(s) were enclosed in a reactor (Swinnex filter holder 13 mm), between two millipore filters (PTFE membrane filters from Osmonics, resistant at a pH range of 1–14, with a diameter of 13 mm and pore size of 0.22 μm). The use of such filters ensured that no solid was transferred to the solution. By using a thin layer of solid, the contact between the solid and liquid phase is optimal, therefore the diffusion effect is minimized and mass-transport influence is avoided.

A feed tank, with 2 L capacity, contained the leaching solution. By means of a peristaltic pump the dissolution was circulated from the bottom to the top to prevent unfilled spaces (bubbles of gas) inside the reactor.

At the outlet of the reactor, aliquots were collected periodically for subsequent analysis of the molybdenum concentration. To determine the exact flow rate, both the weight and the collection time of every sample were measured. The samples were then acidified with HNO_3 (Sigma-Aldrich, 69%) and analysed by ICP-MS 7800 from Agilent Technologies. The ICP-MS was calibrated before the analysis by using a set of molybdenum standards (from Inorganic Ventures).

2.3. XPS measurements

A SPECS system equipped with an Al anode XR50 source operating at 150 W and a Phoibos MCD-9 detector was used. All binding energies obtained were precise to within ±0.2 eV. The spectra were recorded at a pressure below 10^{-8} mbar. The XPS spectra were analysed and fitted

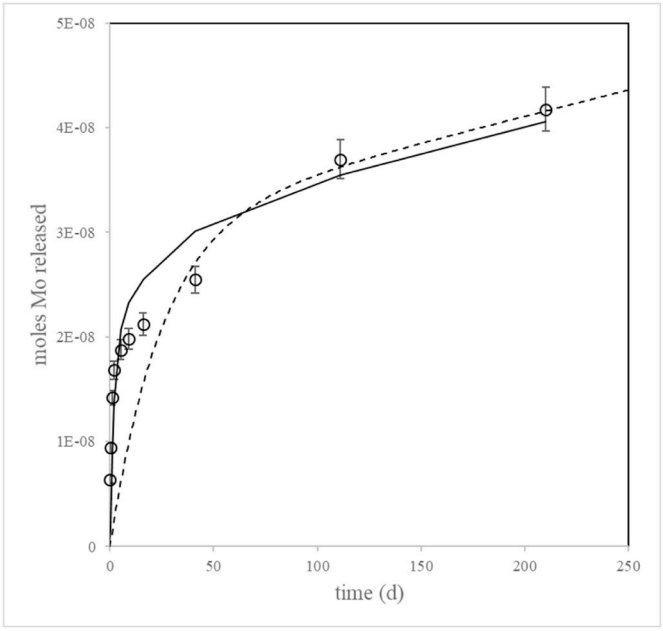

Fig. 1. Molybdenum release as a function of time in the SF dissolution experiments at pH = 8.4. ○ experimental values; dotted line: model considering congruency with uranium; solid line: model considering a fraction of Mo coming from a segregated phase (possibly pre-oxidized molybdenum to Mo(VI)).

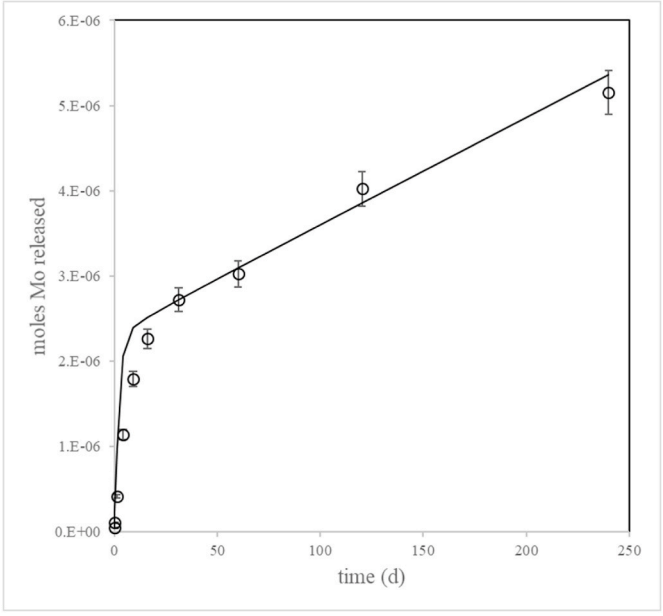

Fig. 2. Molybdenum release as a function of time in the SF dissolution experiments at pH = 13.2. ○ experimental values; solid line: model considering a fraction of molybdenum releasing from a segregated phase.

using CasaXPS software (Casa Software Ltd., UK) version 2.3.25. The spectra were fitted using a 30% of Lorenzian curve and 70% of Gaussian curve with a Shirley background correction. The C 1s, O 1s and Mo 3d orbitals were acquired. Charging effects were corrected by referencing the binding energies to that of O 1s at 530.5 eV, rather than the more usual alignment based on a component within the C 1s spectrum [18].

Molybdenum oxides have been extensively studied by XPS [18–22]. However, the accurate interpretation of the results obtained is a challenge due to the complexity of the XPS spectra, especially when samples contain different oxidation states. The total proportion of each molybdenum oxidation state for Mo oxides (Mo(0), Mo(IV), Mo(V) and Mo(VI)) was calculated by the deconvolution of the Mo 3d spectra, which consisted of a Mo $3d_{5/2}$ – Mo $3d_{3/2}$ doublet for every oxidation state. The relative area ratio between $3d_{5/2}$ and $3d_{3/2}$ doublet was fixed at 3:2 [21]. In addition, the same width (FWHM) and a splitting energy of 3.2 eV were considered for the Mo $3d_{5/2}$ – Mo $3d_{3/2}$ doublet for the fitting [19].

3. Results and discussion

3.1. Spent fuel dissolution

The evolution of the moles of molybdenum released from the SF as a function of time is shown in Figs. 1 and 2. Two different regions can be distinguished, during the first days, there was a relatively high variation of the moles released with time, followed by a slow increase at longer times.

From the comparison of both figures, it was clear that the release of molybdenum was considerably higher at high pH (about two orders of magnitude). This increase in the release of Mo at pH = 13.2 was not particularly surprising, because other radionuclides such as caesium, ruthenium and technetium in the same experiments showed the same behaviour [23].

In order to evaluate the source of the Mo that was being dissolved in each zone, the Segregated Radionuclide Identification and Quantification Model (SERNIM) [11] was fitted to the experimental data in both experiments. The model is able to discriminate between the different possible sources in the fuel where a radionuclide is being released. The general equation of the model for the molybdenum release can be seen in Eq. (1), and it is obtained assuming that Mo is being released through two different sources, the same two sources of uranium release: the pre-oxidized surface of the fuel and the matrix.

$$molMo_t = molMo_{ox,\infty} \cdot \left(1 - e^{-k_{ox} \cdot t}\right) + molMo_{ma,\infty} \cdot \left(1 - e^{-k_{ma} \cdot t}\right) \quad (1)$$

Where $molMo_t$ is the number of cumulative moles of molybdenum released at time t, $molMo_{ox,\infty}$ and $molMo_{ma,\infty}$ are the number of moles contained in the initially oxidized phase and in the matrix, respectively; and k_{ox} and k_{ma} (in d^{-1}) are the rate constants for the release of Mo from the initially oxidized phases and the matrix, respectively. The total moles of molybdenum in the segments used in the experiments might be calculated from the inventory of molybdenum in the fuel (H_{Mo}, 5418 μgMo/gSF, determined with the KORIGEN code), Mo atomic weight (MW) and the weight of the segment (m_{SF}). The moles of Mo in the matrix might be related to the moles contained in the initial oxidized phases according to Eq. (2).

$$molMo_{ma,\infty} = molMo_{SF} - molMo_{ox,\infty} = \frac{m_{SF} \cdot H_{Mo}}{MW} - molMo_{ox,\infty} \quad (2)$$

In the experiment at pH = 8.4 (Fig. 1), the dashed line represents the model obtained assuming that molybdenum released congruently with uranium. As it can be seen, the model seems to fit well to the experimental data after 50 days, but before this time, Mo moles actually released are higher than the predicted by the model. This difference could be the consequence of the release of Mo not only from the uranium pre-oxidized phases and from the matrix, but from an additional source, e.g. Mo oxidized to Mo(VI) in the fuel surface before the start of the experiments. This additional source should be included in the model to obtain Eq. (3).

$$\begin{aligned} molMo_t = {} & molMo_{ox,\infty} \cdot \left(1 - e^{-k_{ox} \cdot t}\right) + molMo_{ma,\infty} \cdot \left(1 - e^{-k_{ma} \cdot t}\right) \\ & + molMo_{seg,\infty} \cdot \left(1 - e^{-k_{seg} \cdot t}\right) \end{aligned} \quad (3)$$

where $molMo_{seg,\infty}$ is the number of Mo moles contained in the segregated phase and k_{seg} (d^{-1}) the rate constant for the release of Mo from the segregated phase. In addition, the total moles of molybdenum in the segments used in the experiments should be recalculated considering

Table 3
Parameters obtained for the fitting of the SERNIM to the molybdenum dissolution experimental data.

	No segregated Mo pH = 8.4	Fraction of segregated Mo pH = 8.4	No segregated Mo pH = 13.2	Fraction of segregated Mo pH = 13.2
$molMo_{ox,\infty}$ ($\pm 10^{-8}$)	$3{\cdot}10^{-8}$	$2{\cdot}10^{-8}$	$3{\cdot}10^{-8}$	$3{\cdot}10^{-8}$
k_{ox} (d^{-1}) (± 0.02)	0.04	0.04	0.04	0.04
$molMo_{ma,\infty}$ ($\pm 1{\cdot}10^{-5}$)	$1.4{\cdot}10^{-4}$	$1.4{\cdot}10^{-4}$	$1.4{\cdot}10^{-4}$	$1.4{\cdot}10^{-4}$
k_{ma} (d^{-1})	$3(\pm 1){\cdot}10^{-7}$	$3(\pm 1){\cdot}10^{-7}$	$9(\pm 1){\cdot}10^{-5}$	$9(\pm 1){\cdot}10^{-5}$
$molMo_{seg,\infty}$		$(2.0 \pm 0.5){\cdot}10^{-8}$		$(2.3 \pm 0.5){\cdot}10^{-6}$
k_{seg} (d^{-1}) (± 0.1)		0.5		0.5

this new term, Eq. (4).

$$molMo_{ma,\infty} = molMo_{fuel} - molMo_{ox,\infty} - molMo_{seg,\infty} \quad (4)$$

In Fig. 1, the solid line represents the moles determined by the SERNIM using Eq. (3). The parameters of the fitting are shown in Table 3, the best fitting was obtained assuming that $2{\cdot}10^{-8}$ mol of Mo were in the segregated phase, which dissolves at a relatively high rate (k_{seg} = 0.5 d^{-1}). The high dissolution rate would indicate that the segregated phase could consist of a fraction of Mo(VI) that could have been formed at the surface during the handling of the fuel, as it was already observed in the literature [5].

The percentage of Mo in the segregated phase might be calculated as the Cumulative Fraction of the Inventory in the Aqueous Phase, $CFIAP_{Mo,seg}$, Eq. (5).

$$CFIAP_{Mo,seg} = \frac{m_{Mo,seg}}{m_{Mo,SF}} \cdot 100 = \frac{molMo_{seg,\infty} \cdot MW}{m_{SF} \cdot H_{Mo}} \cdot 100 \quad (5)$$

Where $m_{Mo,seg}$ and $m_{Mo,SF}$ are the weight of Mo in the segregated phase and in the SF segment, respectively. The value obtained, 0.02% is lower than the values determined for cladded segments of different spent fuels dissolved at pH = 8.3 in previous works: 0.11% [10] and 0.30% [24].

After the relatively fast initial dissolution, the release of molybdenum was congruent with uranium, and the long-term molybdenum release rate was $3.6{\cdot}10^{-10}$ mol m^{-2} s^{-1}, a similar value to the one obtained using continuous flow-through experiments with spent fuel in 10 mM $NaHCO_3$ solutions under oxidizing conditions, $3.0{\cdot}10^{-10}$ mol m^{-2} s^{-1} for ^{100}Mo [25].

Fig. 2 shows, on the other hand, the fitting of the experimental data by the model at pH = 13.2 considering the three contributions and the expression of the model according to equation (3). In this case, the fitting considering congruent release with uranium is not included because it resulted always in much lower molybdenum cumulative moles released (lower than 10^{-7}). The parameters of the fitting are shown in Table 3 and for the initial release of molybdenum the value of $molMo_{seg,\infty}$ was increased more than two orders of magnitude, indicating that during this step a high amount of molybdenum was being released from a source other than the pre-oxidized to Mo(VI) considered at pH = 8.4.

In addition, the fitting after the initial Mo release was obtained also with a higher k_{ma} value, giving a long-term Mo release rate of $4.6{\cdot}10^{-8}$ mol m^{-2} s^{-1} which is, as far as we know, the first Mo release rate published at high alkaline pH. A CFIAP of 5.4% was calculated from Eq. (5), a value much higher than the obtained at pH = 8.4, 0.02%. In addition, the IRF for Mo might be calculated from eq. (6).

$$IRF = CFIAP_{Mo,seg} - CFIAP_{U} \quad (6)$$

where $CFIAP_U$ is the Fraction of Inventory in the Aqueous Phase for uranium (data taken from Ref. [23]). The IRF obtained was 5.3%, indicating a very important contribution of Mo to the IRF under these conditions, with much higher values than the calculated at slightly alkaline pH for different fuels in the literature: 0.01–0.4% [6,7,9,10].

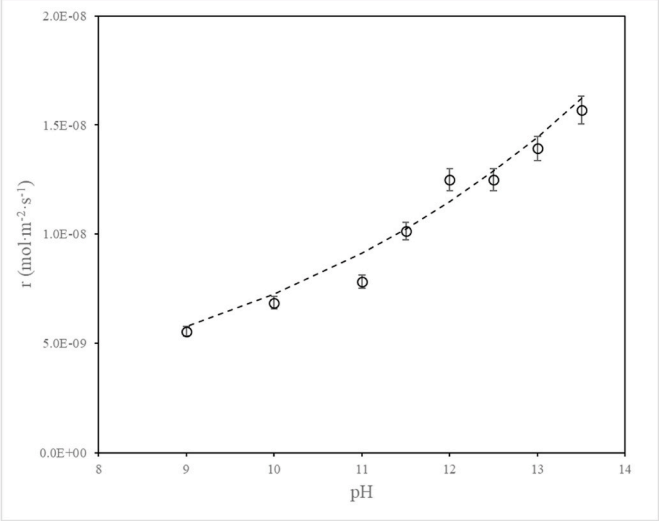

Fig. 3. Normalized dissolution rates of Mo(s) as a function of pH obtained from the flow-through experiments. The dotted line represents the fitting of Eq. (8).

The main conclusion from the experimental data and the fitting of the model is that at pH = 13.2 there was an additional source of molybdenum to the uranium-related sources and the pre-oxidized Mo(VI) on the surface. Considering the distribution of Mo in the fuel, the higher release of molybdenum at more alkaline pH could be related to the dissolution of metallic particles that are present in the fuel at (1) the grain boundaries (that would affect to the release of Mo during the first dissolution step), and (2) inside the fuel grains (affecting to the long-term Mo release).

3.2. Dissolution of Mo(s) at alkaline pH

In order to know if the high increase in the release of molybdenum from SF at high pH is due to the dissolution of metallic particles, the Mo (s) dissolution rate was determined in a pH range of 9–13.5 using a thin solid layer flow-through reactor. From the molybdenum concentrations measured at the outlet of the reactor, the normalized dissolution rate could be calculated according to Eq. (7).

$$r_{diss}\left(mol \cdot m^{-2} \cdot s^{-1}\right) = \frac{Q \cdot [Mo]}{SA \cdot m} \quad (7)$$

Where Q is the flow rate ($m^3{\cdot}s^{-1}$), [Mo] is the molybdenum concentration of the effluent once steady state was reached ($mol{\cdot}m^{-3}$), SA is the surface area of the solid (m^2/g) and m is the mass of the solid enclosed in the reactor (g).

The dissolution rates obtained are shown in Fig. 3 and the main trend is that dissolution rate increased with pH. This dependence can be expressed according to Eq. (8).

$$r_{diss}\ (mol{\cdot}s^{-1}\ m^{-2}) = 10^{-9{,}14\ (\pm 0{,}06)} \cdot [H^+]^{-0{,}10\ (\pm 0{,}01)} \quad (8)$$

The negative dependence of the dissolution rate on proton concentration evidences that the dissolution rate is promoted by the presence of OH^- ions in the solution. In addition, a fractional order dependence on proton concentration is commonly seen in surface complexation-promoted reactions for minerals dissolution, including oxides [26]. Consequently, the variation of the Mo(s) dissolution rate with pH could be explained as the consequence of a hydroxyl-promoted dissolution, whereas the fractional rate order points to a dissolution promoted by a surface complexation mechanism.

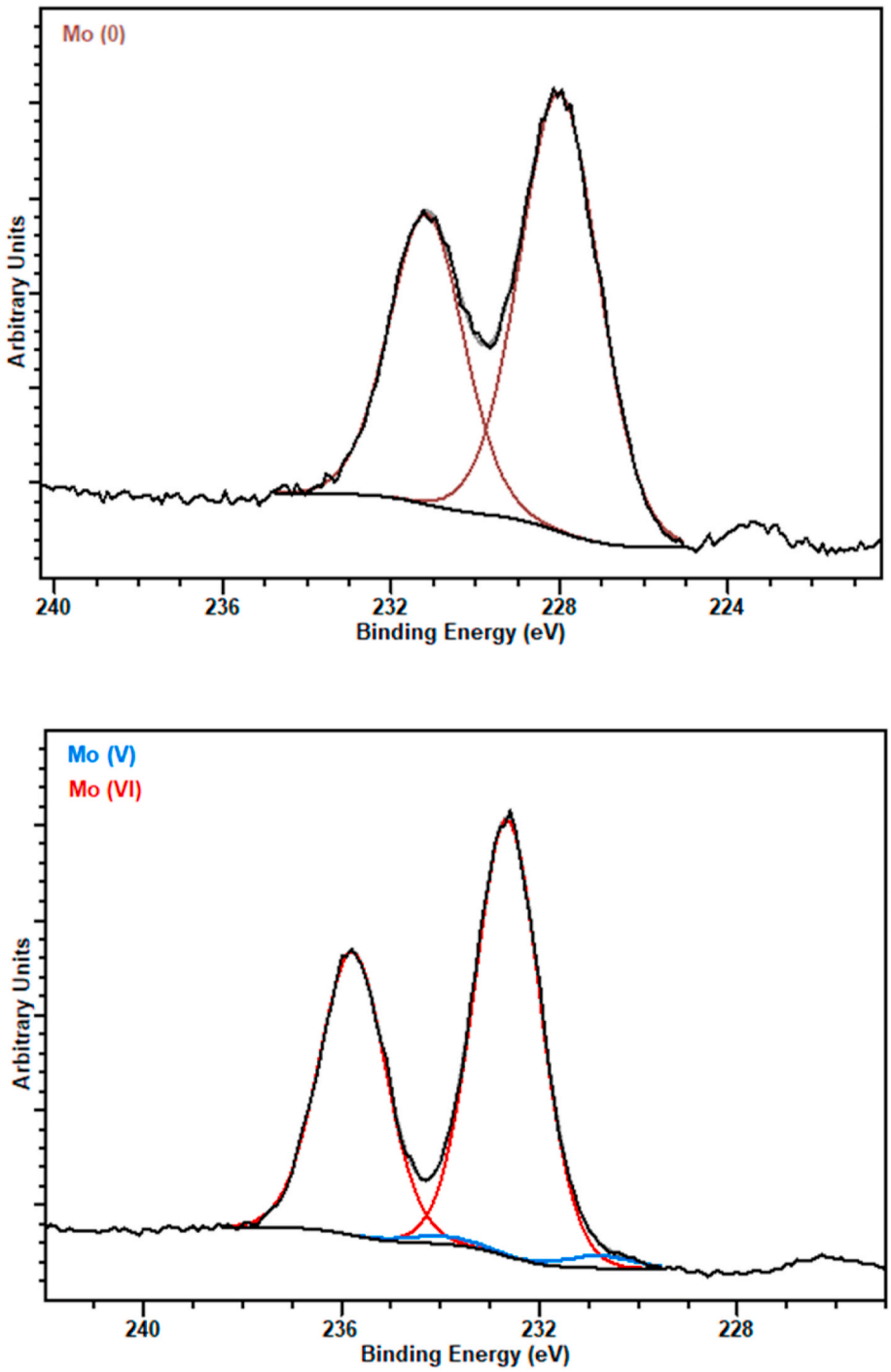

Fig. 4. Mo 3d XPS spectra of the Mo(s) (up) and MoO_3(s) (down) solids used as patterns.

The higher release of Mo from SF observed at hyperalkaline pH (almost two orders of magnitude higher than at alkaline pH) could, therefore, be attributed to the higher dissolution rate of Mo(s). Molybdenum release rates in the experiment with SF ($4.6{\cdot}10^{-8}$ mol m^{-2} s^{-1}) and with Mo(s) ($1.5{\cdot}10^{-8}$ mol m^{-2} s^{-1}) are of the same order of magnitude, in spite of the different experimental setup and, especially, the morphology of the solid used in both experiments.

Considering the Mo(s) dissolution rates obtained in this work, the increase of the Mo release in the SF dissolution experiment at high pH might be related to the higher dissolution of Mo(s) in the metallic inclusions in the fuel. An increase in the dissolution rate of metals (including noble metals) was previously described at alkaline pH [27, 28]. This increase was explained considering that the oxidation of the metal to the thermodynamically stable oxide phases went through the formation of intermediate oxides on the surface of the metals with relatively fast dissolution rates. These phases would start to dissolve before the formation of the stable oxide, resulting in a dissolution higher than expected considering only the solubility of the stable solid phase.

In the case of molybdenum, some authors proposed that the process of Mo(s) oxidation and subsequent dissolution occurred through the formation of intermediate species with different Mo oxidation states. Saji and Lee [29] proposed a mechanism of Mo(s) oxidation to Mo(VI) and the release of MoO_4^{2-} to the aqueous phase promoted by the OH^- ion and including Mo(III) transition phases on the solid surface such as > Mo

Table 4
XPS results for patterns and for the solids at the end of two experiments. The Mo(s) pattern was the solid used at the start of the experiments.

Sample	BE Mo $3d_{5/2}$ (eV)				%Mo (±5)			
	Mo(0)	Mo(IV)	Mo(V)	Mo(VI)	Mo(0)	Mo(IV)	Mo(V)	Mo(VI)
MoO_3 pattern	–	–	230.8	232.6	–	–	2.9	97.1
Mo(s) pattern	228	–	–	–	100	–	–	–
Mo(s) (pH10)	228.3	229.2	230.7	232.7	1.7	45.6	24.5	28.2
Mo(s) (pH13.5)	228.3	229.3	230.8	232.7	0.7	21.8	14.1	63.4

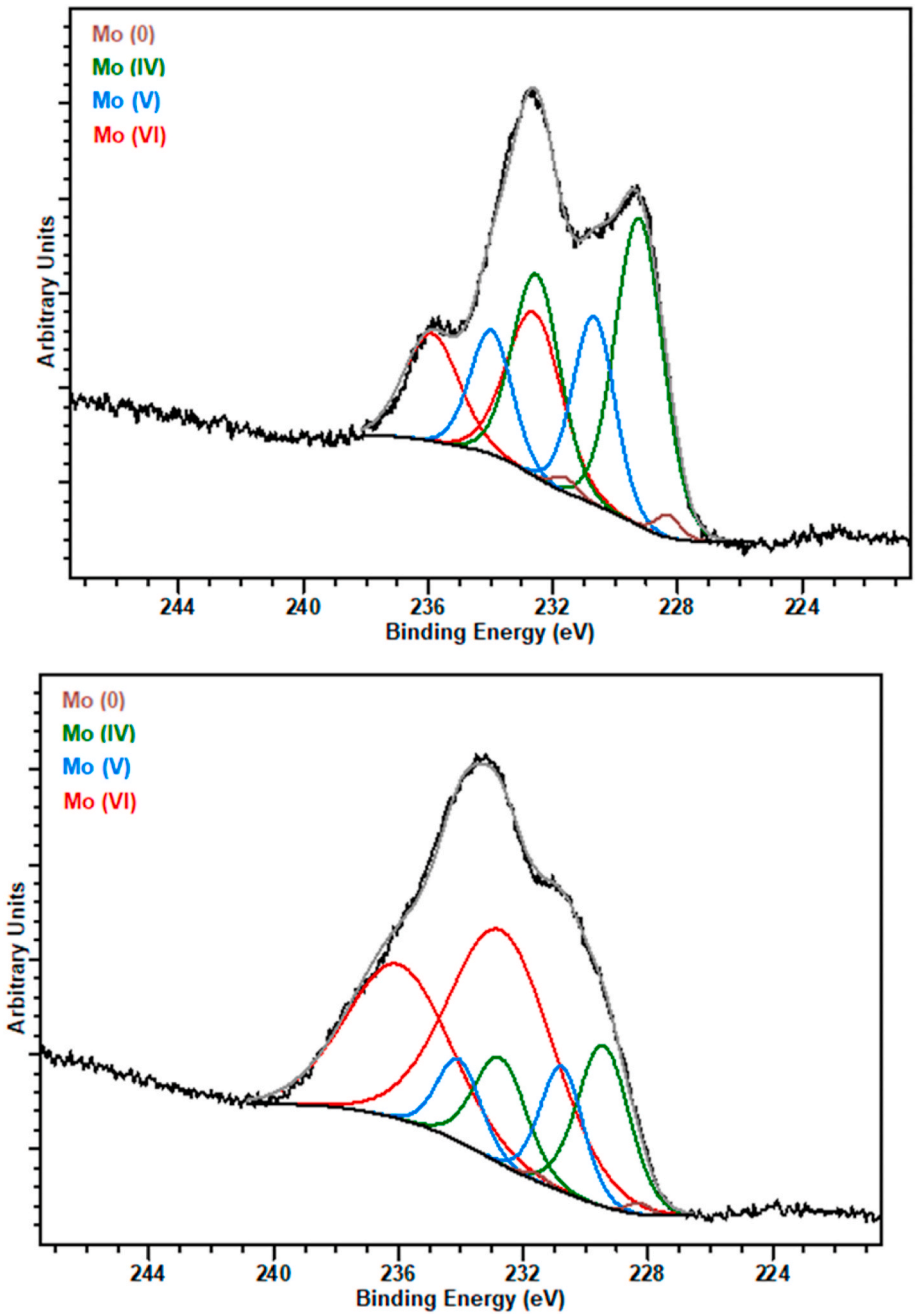

Fig. 5. Mo 3d XPS spectra resolved into Mo(0), Mo(IV), Mo(V) and Mo(VI) contributions, recorded after experiments at pH 10 (up) and pH 13.5 (down).

$(OH)_2^+$ and $>Mo(OH)_3$. In a slightly alkaline pH, Petrova et al. [30] proposed that in the oxidation of Mo(s) to Mo(VI), intermediate Mo(V) surface complexes promoted by the OH^- are formed on the surface of the solids that were dissolving in parallel with Mo(VI) release to the solution.

3.3. XPS results of non irradiated Mo(s) during the dissolution experiments

In order to get more evidence on the mechanism that could induce a higher dissolution of Mo(s) in alkaline media, the solids at the end of two

experiments were analysed by XPS, which permitted to determine the molybdenum oxidation state on the surface.

For the determination of the Mo oxidation state in the experiments carried out in this work, two different patterns were used: Mo(s) and MoO_3(s), whose spectra are shown in Fig. 4. In the case of Mo(s), two well-resolved peaks with a binding energy of 228.0 eV for Mo $3d_{5/2}$ were assigned to Mo(0) [31] with a splitting energy of 3.2 eV and a FWHM of 2.0 eV.

The spectrum of MoO_3 showed the presence of two well-resolved peaks at 232.5 and 235.6 eV (FWHM of 1.6 eV), which were assigned to the Mo $3d_{5/2}$ and Mo $3d_{3/2}$ spin-orbit components, respectively. These values agreed with the ones reported in the literature [17,18,20,32,33]. In addition, a weak doublet shifted 1.7 eV to lower binding energy was assigned to Mo(V) at 230.8 and 234.0 eV [34], indicating that the sample was not completely oxidized to Mo(VI).

The XPS binding energies of Mo 3d spectra for patterns and for the solids in the experiments, as well as the percentage contributions of Mo (0), Mo(IV), Mo(V) and Mo(VI), are summarized in Table 4, while Fig. 5 shows the XPS spectra of the surface of Mo(s) at the end of the experiments at two different pH values, 10 and 13.5. The value of the percentage of each molybdenum oxidation state was determined from the deconvolution of the Mo 3d peak into 8 peaks, with Mo $3d_{5/2}$ peaks of Mo(0) (228.3 eV), Mo(IV) (229.2 eV), Mo(V) (230.6 eV) and Mo(VI) (232.7 eV). According to the literature, the Mo $3d_{5/2}$ peak binding energies corresponding to the oxidation states Mo (0), Mo (IV) and Mo(VI) are located at 228.3 eV, 229.1–229.3 eV and 232.5 eV, respectively [21].

As it can be seen in Table 4, in both cases the surface was oxidized, but at pH = 10 the predominant oxidation state was IV while at pH = 13.5 was VI. The oxidation of Mo(s) to Mo(VI) at pH = 13.2 (more than 60% of the Mo(s) surface was oxidized to Mo(VI) at this pH) would be responsible of the higher dissolution rate, while a proportion of Mo oxidized to Mo(VI) should not be discarded even at pH = 10. The composition of the surface of the solid at the end of the experiments also showed intermediate Mo oxidation states (IV and V) which could also contribute at high pH to the release of Mo to the solution causing a faster dissolution rate in alkaline media.

4. Conclusions: Release of molybdenum from SF

From the results obtained in this work, the complexity of the release of molybdenum produced by fission processes is better understood. It seems to involve at least three different oxidation states and three different localizations in the fuel that are responsible for the net molybdenum release to the solutions as a function of time, without considering other possible sources of Mo as the cladding itself and the crud on the cladding.

At slightly alkaline pH, the initial release of Mo is mainly due to Mo (IV) contained in uranium pre-oxidized phases and fines, but also from a fraction of molybdenum that could have been oxidized to Mo(VI) before the start of the experiment. This fraction of Mo(VI) would represent approximately only 0.02% of the total molybdenum in the fuel but it is particularly important because it would be a part of the IRF. After the dissolution of both the preoxidized uranium phases and Mo(VI) on the surface of the SF, molybdenum released to the solution would be mainly coming from Mo(IV) situated in the UO_2 lattice. A small fraction could also be coming from Mo(s) metallic particles through an oxidative dissolution mechanism, although a relatively low oxidative dissolution rate would be expected at this pH.

On the other hand, at high alkaline pH, the behaviour is different mainly because of the faster oxidation of Mo(s) to Mo(VI) resulting in a higher release of Mo to the solution. During the first days, the Mo release would be very high compared to pH = 8.4 due to the dissolution of Mo(s) particles, which are oxidized from Mo(0) to Mo(VI), as it was deduced from the XPS results. The high Mo concentrations in solution during the first days would therefore mainly be the consequence of the dissolution of Mo from metallic particles in the voids and in the grain boundaries. At long-term, the Mo released to the solution would come from two different sources in the fuel, on one hand from the Mo(IV) in the UO_2 lattice and, on the other hand, from the intragranular metallic particles.

This study of the Mo chemistry and its release from the SF might help tu understand the description of the fuel oxidation and dissolution and, therefore, the release of radionuclides.

Declaration of competing interest

The authors declare that they have no known competing financial interests or personal relationships that could have appeared to influence the work reported in this paper.

Acknowledgments

This work has been financially supported by Ministerio de Economía y Competitividad (Spain) with the project PID2020-116839RB-I00 and ENRESA (Empresa Nacional de Residuos Radioactivos de España) under CO-IA-22-010 and ENRESA/JRC/Eurecat 33924 agreement. Finantial support is also acknowledged to The Agency for Business Competitiveness (ACCIÓ) and the European Union's European Atomic Energy Community's (Euratom) Horizon 2020 Reasearch and Training Programme (H2020-NFRP-2016-2017-1), section B - Contribute to the Development of Solutions for the Management of Radioactive Waste, topic NFRP 6: Addressing key priority R&I issues for the first-of-the-kind geological repositories under grant agreement n° 755443 (Modern Spent Fuel Dissolution and Chemistry in Failed Container Conditions, DisCo project). S. G.-G. wants to acknowledge the fellowship with reference code PRE2018–085618 and J.L. is a Serra Hunter Fellow and is grateful to the ICREA Academia program.

References

[1] Y.K. Ha, J.G. Kim, Y.S. Park, S.D. Park, K. Song, Behavior of molybdenum in UO_2 fuel matrix, Nucl. Eng. Technol. 43 (2011) 309–316.
[2] H. Kleykamp, The chemical state of the fission products in oxide fuels, J. Nucl. Mater. 131 (1984) 221–246.
[3] S. Nicoll, Hj. Matzke, R.W. Grimes, C.R.A. Catlow, The behaviour of single atoms of molybdenum in urania, J. Nucl. Mater. 240 (1997) 185–195.
[4] L. Desgranges, B. Pasquet, M. Fraczkiewicz, Interpretation of the molybdenum behaviour in irradiated UO_2 using a point defect approach, Nucl. Instrum. Methods Phys. Res. B 266 (2008) 3018–3022.
[5] P. Martin, M. Ripert, G. Carlot, Ph. Parent, C. Laffon, A study of molybdenum behaviour in UO_2 by X-ray absorption spectroscopy, J. Nucl. Mater. 326 (2004) 132–143.
[6] A. Martínez-Torrents, D. Serrano-Purroy, I. Casas, J. De Pablo, Influence of the interpellet space to the instant release fraction determination of a commercial UO_2 boiling water reactor spent nuclear fuel, J. Nucl. Mater. 499 (2018) 9–17.
[7] D. Serrano-Purroy, I. Casas, E. González-Robles, J.-P. Glatz, D. Wegen, F. Clarens, J. Giménez, J. de Pablo, A. Martínez-Esparza, Dynamic leaching studies of 48 MWd/kgU UO_2 commercial spent nuclear fuel under oxic conditions, J. Nucl. Mater. 434 (2013) 451–460.
[8] E. González-Robles, D. Serrano-Purroy, R. Sureda, I. Casas, J. de Pablo, Dissolution experiments of commercial PWR (52 MWd/kgU) and BWR (53 MWd/kgU) spent nuclear fuel cladded segments in bicarbonate water under oxidizing conditions. Experimental determination of matrix and instant release fraction, J. Nucl. Mater. 465 (2015) 63–70.
[9] D. Serrano-Purroy, I. Casas, E. González-Robles, J.-P. Glatz, D. Wegen, F. Clarens, J. Giménez, J. de Pablo, A. Martínez-Esparza, Instant release fraction and matrix release of high burn-up UO_2 spent nuclear fuel: effect of high burn-up structure and leaching solution composition, J. Nucl. Mater. 427 (2012) 249–258.
[10] A. Martínez-Torrents, D. Serrano-Purroy, R. Sureda, I. Casas, J. de Pablo, Instant release fraction corrosion studies of commercial UO2 BWR spent nuclear fuel, J. Nucl. Mater. 488 (2017) 302–313, https://doi.org/10.1016/j.jnucmat.2017.03.022.
[11] A. Espriu-Gascon, A. Martínez-Torrents, D. Serrano-Purroy, J. Giménez, J. de Pablo, I. Casas, Contribution of phases segregated from the UO_2 matrix to the release of radionuclides from spent nuclear fuel and duration of the Instant Release Fraction (IRF), J. Nucl. Mater. 532 (2020), 152066.
[12] I. Pointeau, C. Landesman, E. Giffaut, P. Reiller, Reproducibility of the uptake of U (VI) onto degraded cement pastes and calcium silicate hydrate phases, Radiochim. Acta 92 (2004) 645.
[13] E. Wieland, C.A. Johnson, B. Lothenbach, F. Winnefeld, Mechanisms and modelling of waste/cement interactions – survey of topics presented at the Meiringen Workshop, Mater. Res. Soc. Symp. Proc. 932 (2006) 663.

[14] T. Heath, J. Schofield, A. Shelton, Understanding cementitious backfill interactions with groundwater components," Appl, Geochemistry 113 (2019), 104495.
[15] L. Wang, Near-field chemistry of a HLW/SF repository in Boom Clay - scoping calculations relevant to the supercontainer design, in: External Report of the Belgian Nuclear Research Centre, SCK-CEN, 2009.
[16] M.R. Savina, B.H. Isselhardt, D.Z. Shulaker, M. Robel, A.J. Conant, B.J. Ade, Simultaneous isotopic analysis of fission product Sr, Mo, and Ru in spent nuclear fuel particles by resonance ionization mass spectrometry" Nature, Sci. Rep. 13 (2023) 5193.
[17] J. Bruno, I. Casas, I. Puigdomènech, The kinetics of dissolution of UO_2 under reducing conditions and the influence of an oxidized surface layer (UO_{2+x}): application of a continuous flow-through reactor, Geochim. Cosmochim. Acta 55 (1991) 647–658.
[18] J. Baltrusaitis, B. Mendoza-Sanchez, V. Fernandez, R. Veenstra, N. Dukstiene, A. Roberts, N. Fairley, Generalized molybdenum oxide surface chemical state XPS determination via informed amorphous sample model, Appl. Surf. Sci. 326 (2015) 151–161.
[19] J.G. Choi, L.T. Thompson, XPS study of as-prepared and reduced molybdenum oxides, Appl. Surf. Sci. 93 (1996) 143–149.
[20] O. Marin-Flores, L. Scudiero, S. Ha, X-ray diffraction and photoelectron spectroscopy studies of MoO_2 as catalyst for the partial oxidation of isooctane, Surf. Sci. 603 (2009) 2327–2332.
[21] D.O. Scanlon, G.W. Watson, D.J. Payne, G.R. Atkinson, R.G. Egdell, D.S.L. Law, Theoretical and experimental study of the electronic structures of MoO_3 and MoO_2, J. Phys. Chem. C 114 (2010) 4636–4645.
[22] P.A. Spevack, N.S. McIntyre, Thermal reduction of MoO_3, J. Phys. Chem. 96 (1992) 9029–9035.
[23] L. Iglesias, J. Kokinda, D. Serrano-Purroy, A. Martínez-Torrens, I. Casas, J. de Pablo, F. Clarens, J. Giménez, "Dissolution of high Burn-Up Spent Nuclear Fuel at high-pH in the presence of calcium and silicon," Submitted to Radiochimica Acta.
[24] Th. Mennecart, Ch. Cachoir, K. Lemmens, Fast release from clad and declad spent UOX PWR fuel segments in a bicarbonate solution under anoxic conditions, J. Nucl. Mater. 557 (2021), 153257.
[25] S. Röllin, K. Spahiu, U.-B. Eklund, Determination of dissolution rates of spent fuel in carbonate solutions under different redox conditions with a flow-through experiment, J. Nucl. Mater. 297 (2001) 231–243.
[26] W. Stumm, R. Wollast, Coordination chemistry of weathering: kinetics of the surface-controlled dissolution of oxide minerals, Rev. Geophys. 28 (1990) 53–69.
[27] M. Schalenbach, O. Kasian, M. Ledendecker, F.D. Speck, A.M. Mingers, K.J. J. Mayrhofer, S. Cherevko, The electrochemical dissolution of noble metals in alkaline media, Electrocatalysis 9 (2018) 153–161.
[28] S. Cherevko, A.R. Zeradjanin, G.P. Keeley, K.J.J. Mayrhofer, A Comparative study on gold and platinum dissolution in acidic and alkaline media, J. Electrochem. Soc. 161 (2014) H822–H830.
[29] V.S. Saji, Ch.-W. Lee, Molybdenum, molybdenum oxides, and their electrochemistry, ChemSusChem 5 (2012) 1146–1161.
[30] M. Petrova, M. Bojinov, S. Zanna, Ph. Marcus, Mechanism of anodic oxidation of molybdenum in nearly-neutral electrolytes studied by electrochemical impedance spectroscopy and X-ray photoelectron spectroscopy, Electrochim. Acta 56 (2011) 7899–7906.
[31] D. Briggs (Chapter 22) "X-ray Photoelectron Spectroscopy", in: D.E. Packham (Ed.), Handbook of Adhesion, second ed., John Wiley & Sons, Ltd, 2005.
[32] C.D. Wagner, W.M. Riggs, L.E. Davis, J.F. Moulder, G.E. Mullenberg, Handbook of X-Ray Photoelectron, Spectroscopy" Perkin-Elmer Corporation Publ., USA), 1979.
[33] B. Mendoza-Sánchez, T. Brousse, C. Ramirez-Castro, V. Nicolosi, P.S. Grant, An investigation of nanostructured thin film α-MoO_3 based supercapacitor electrodes in an aqueous electrolyte, Electrochim. Acta 91 (2013) 253–260.
[34] F. Nacimiento, M. Cabello, R. Alcántara, C. Pérez-Vicente, P. Lavela, J.L. Tirado, Exploring an aluminum ion battery based on molybdite as working electrode and ionic liquid as electrolyte, J. Electrochem. Soc. 165 (2018) A2994–A2999.